molecules

MDPI

Article

Computational Study of the Kinetics and Mechanisms of Gas-Phase Decomposition of *N*-Diacetamides Using Density Functional Theory

Oswaldo Luis Gabidia Torres [1,*], Marcos Loroño [1,*], Jose Luis Paz Rojas [2], Cecilio Julio Alberto Garrido Schaeffer [3], Thais Cleofe Linares Fuentes [4] and Tania Cecilia Cordova Sintjago [5]

1 Departamento Académico de Fisicoquímica, Facultad de Química e Ingeniería Química, Universidad Nacional Mayor de San Marcos, Lima 15081, Peru
2 Departamento Académico de Química Inorgánica, Facultad de Química e Ingeniería Química, Universidad Nacional Mayor de San Marcos, Lima 15081, Peru; jpazr@unmsm.edu.pe
3 Departamento Académico de Operaciones Unitarias, Facultad de Química e Ingeniería Química, Universidad Nacional Mayor de San Marcos, Lima 15081, Peru; cgarridos@unmsm.edu.pe
4 Departamento Académico de Química Orgánica, Facultad de Química e Ingeniería Química, Universidad Nacional Mayor de San Marcos, Lima 15081, Peru; tlinaresf@unmsm.edu.pe
5 Department of Natural Sciences, Santa Fe College, Gainesville, FL 32066, USA; tania.cordova-sintjago@sfcollege.edu
* Correspondence: oswaldo.gabidia@unmsm.edu.pe (O.G.T.); mloronog@unmsm.edu.pe (M.L.)

Abstract: In this research work, we examined the decomposition mechanisms of *N*-substituted diacetamides. We focused on the substituent effect on the nitrogen lone-pair electron delocalization, with electron-withdrawing and electron donor groups. DFT functionals used the following: B1LYP, B3PW91, CAMB3LYP, LC-BLYP, and X3LYP. Dispersion corrections (d3bj) with Becke–Johnson damping were applied when necessary to improve non-covalent interactions in the transition state. Pople basis sets with higher angular moments and def2-TZVP basis sets were also applied and were crucial for obtaining consistent thermodynamic parameters. The proposed mechanism involves a six-membered transition state with the extraction of an α hydrogen. Several conformers of *N*-diacetamides were used to account for the decrease in entropy in the transition state in the rate-determining state. All calculations, including natural bond orbital (NBO) analyses, were performed using the Gaussian16 computational package and its GaussView 6.0 visualizer, along with VMD and GNUPLOT software. The isosurfaces and IBSIs were calculated using MultiWFN and IGMPlot, respectively.

Keywords: DFT; diacetamides; pyrolysis; IBSI; NBO; reaction mechanism

check for updates

Citation: Gabidia Torres, O.L.; Loroño, M.; Paz Rojas, J.L.; Garrido Schaeffer, C.J.A.; Linares Fuentes, T.C.; Cordova Sintjago, T.C. Computational Study of the Kinetics and Mechanisms of Gas-Phase Decomposition of *N*-Diacetamides Using Density Functional Theory. *Molecules* **2024**, *29*, 3833. https://doi.org/10.3390/molecules29163833

Academic Editors: Aurora Costales and Fernando Cortés-Guzmán

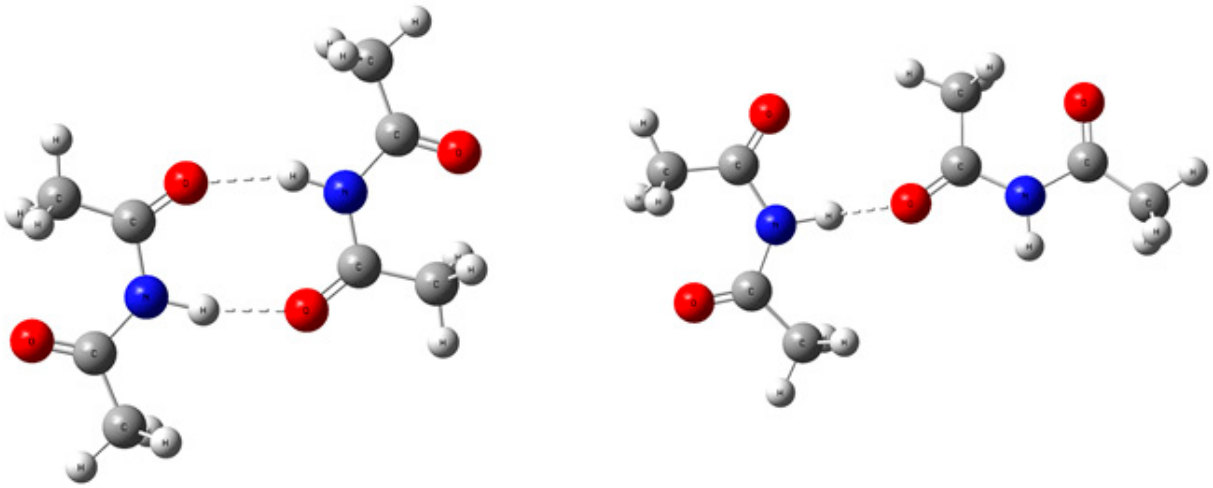
Received: 16 July 2024
Revised: 5 August 2024
Accepted: 6 August 2024
Published: 13 August 2024

Copyright: © 2024 by the authors. Licensee MDPI, Basel, Switzerland. This article is an open access article distributed under the terms and conditions of the Creative Commons Attribution (CC BY) license (https://creativecommons.org/licenses/by/4.0/).

1. Introduction

Diacetamide and *N*-acetyl acetamide ($CH_3CONHCOCH_3$) exist as dimers in a crystalline state. The molecules are bound via hydrogen bonding C=O---HN, in which one carbonyl group of the molecule acts as a proton acceptor for the imide proton, while the other carbonyl group is not bound by hydrogen at all [1–4]. Due to this intermolecular hydrogen bonding, the geometry of diacetamides shows small differences in their structures when comparing the gas phase and X-ray electron diffraction geometries. The intramolecular hydrogen bonds C=O---HN cause an elongation of the C=O bond (0.01 Å) and a comparable shortening of the CN bond with respect to the values of the isolated molecule [5]. Figure 1 shows two models. In the first model (Figure 1a), an HN bond reproduces the cyclic dimer of the crystal. The second model (Figure 1b) describes a structure where two monomers are associated by a single C=O---HN hydrogen bond and form an open dimer structure. The latter model describes a disordered intermolecular interaction like that expected in a concentrated low-temperature matrix. Gas-phase electron diffraction

also suggests that this diacetamide is a nearly planar molecule with a thermally averaged dihedral angle between the two acetyl groups of 36° [5,6].

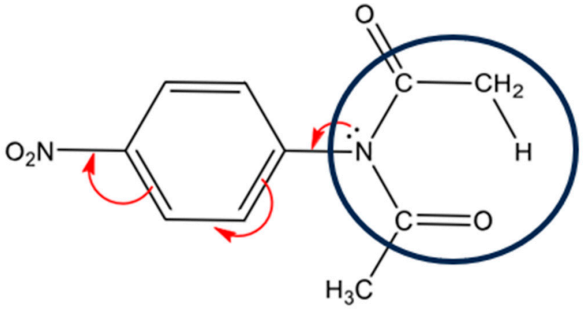


(**a**) (**b**)

Figure 1. (**a**) C_{2h} and (**b**) C_s symmetry structures of diacetamide dimers and HF/6-31G geometry of the hydrogen bonds (bond distances in Å and bond angles in degrees), as shown in reference [5].

It is generally accepted that the hydrolysis of acetamide is initiated by the formation of an *O*-protonated tautomer through the nucleophilic attack of a water molecule on carbonyl oxygen. However, the homogeneous gas-phase pyrolysis of acetamide produces ammonia (NH_3), acetic acid (CH_3COOH), and acetonitrile (CH_3CN) as the main products. Alternate decarboxylation and dehydration reaction pathways were suggested, which dominate the unimolecular breakdown of analog acetic acid. Ammonia, acetic acid, and acetonitrile are also the main products of acetamide hydrolysis in supercritical water and during photodissociation [7]. One of the techniques used to study molecular decompositions is pyrolysis. The molecules are known to have limited thermal stability, which leads to the formation of smaller molecules, although the resulting fragments can also interact and generate larger compounds compared to the initial molecule. When the heating temperature is above 350 °C, chemical processes caused by thermal energy alone are called pyrolysis (Py). Chemical reactions caused by heat at lower temperatures (e.g., 250 °C) are called thermal decompositions [8–11]. Numerous pyrolysis products occur in nature; the toxicological and environmental implications of their presence are of considerable interest [12–14].

Scheme 1 shows the proposed mechanism for the thermal decomposition of a *N*-(4-nitrophenyl) diacetamide given by AL-AWADI et al. [15], involving a six-membered ring, where the participation of the lone-paired electrons of nitrogen is very important. The kinetic data revealed that this reaction follows a first-order kinetics. The reactivity is modified when a *N*-aryl substituent is present, relative to a simple diacetamide.



Scheme 1. AL-AWADI proposed a mechanism involving a six-membered transition state (circled). Delocalization of the nitrogen lone pair is shown.

Molecules with a delocalized p-system of electrons represent attractive targets for application in advanced functional materials. These molecules have junctions in which nitrogen actively participates. This work aims to provide more insight into the thermal decomposition of *N*-substituted diacetamides. The effects of substituents at the aromatic ring are discussed. To do so, the thermodynamic properties of diacetamides were computationally determined and then compared with the available experimental data.

2. Computational Methodology

The molecular structure of all compounds in this study, reactant, and products, were optimized at the level of theory used to calculate the thermodynamic parameters. The series includes N-substituted diacetamides, namely $NX(COCH_3)_2$ with X substituents: H, phenyl, or 4-nitrophenyl. These parameters were used to evaluate the kinetics of the decomposition reaction of N-substituted diacetamides and measure the effects of the electron donor and/or electron-withdrawing groups at the substituent on the nitrogen. Table 1 shows only the experimental activation energies obtained by AL-AWADI [15].

Table 1. Experimental activation energies for $NX(COCH_3)_2$ pyrolysis.

X	Ea (kJ mol^{-1})
Hydrogen	151.3 ± 2.7
Phenyl	185.7 ± 7.5
4-nitrophenyl	192.0

The Gaussian16 computational package revision C.01 WIN64-version 1.1 [16] was used in order to carry out all the structure optimizations studied with the following DFT functionals: B1LYP, B3PW91, CAMB3LYP, LC-BLYP, and X3LYP together with the basis sets 6-31+g(d,p), 6-31+(2d,2p) and 6-31+(3df,2p), 6-311+(2d,2p), 6311+(3df, 2p), and def2-TZVP [17,18]. All calculations were carried out to convergence, with no negative frequencies for the minimum energy structures, or a single negative frequency if a transition state is involved. To ensure that there was a correspondence between reactants and products, an intrinsic coordinate interaction (IRC) procedure was used, thus creating an energy interaction coordinate that connected the participating species through the activation energy. The topological properties of the electron density at the bonding critical point (bcp) of molecules were calculated according to Bader's quantum theory of atoms in molecules (AIM). The reduced density gradient was obtained to determine the types of non-covalent interactions present in the structure. These calculations were carried out using the MultiWFN software [19]. To measure the strength of the bonds, the independent gradient model (IGM) was used [20–25]. Finally, frequency calculations allowed for obtaining zero-point vibrational energy (ZPVE), temperature corrections [E(T)], and absolute entropies [S(T)] assuming ideal gas behavior from the harmonic frequencies and moments of inertia by standard methods [26]. The Gibbs free energy change ($\Delta G^{\#}$) between each reactant (R) and its transition state (TS), was estimated using the following equations:

$$\Delta G^{\#} = \Delta H^{\#} - T\Delta S^{\#} \quad (1)$$

$$\Delta H^{\#} = V^{\#} + \Delta ZPVE + \Delta E(T) \quad (2)$$

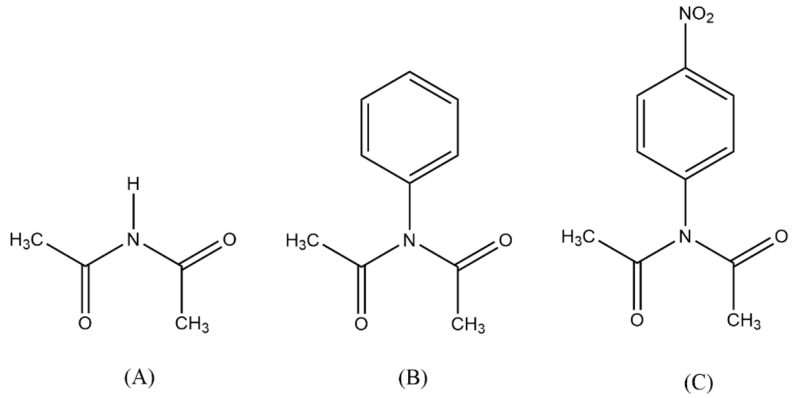
where $V^{\#}$ is the potential energy barrier and $\Delta ZPVE$ and $\Delta E(T)$ are the differences in ZPVE and temperature corrections between the TS and the R, respectively. Entropy values were estimated from a harmonic vibrational analysis.

3. Results and Discussion

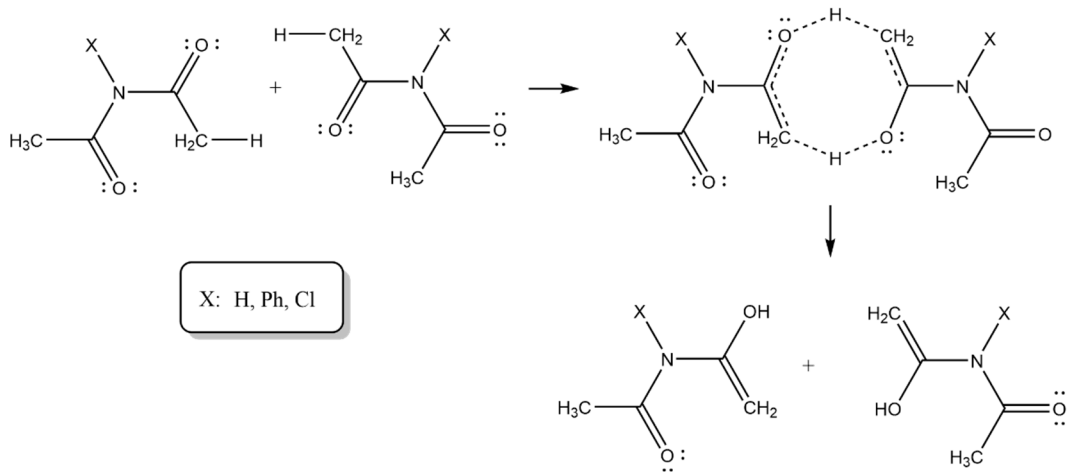
The experimental results given by AL-AWADI entail a six-membered ring transition state, where an α hydrogen is extracted by the carbonyl oxygen; see Scheme 1. According to Table 1, if X=H, the activation energy is 151.3 ± 2.7 kJ/mol; it rises significantly when

hydrogen is substituted by a phenyl group or substituted up to an average energy of 190 kJ/mol. The effect is explained by a delocalization of electrons from nitrogen to the phenyl group. This energy difference is about 40 kJ/mol. This increase in energy can be explained computationally, making use of the density functional theory (DFT). For this purpose, several types of functionals—B3PW91, X3LYP, B1LYP, LC-BLYP, and CAM-B3LYP—and different Pople basis sets—with dispersion corrections and Becke–Johnson damping (d3bj)—were chosen. Additionally, an Ahlrichs def2-TZVP basis set was also used.

Three compounds were analyzed together with three possible mechanisms, $NX(COCH3)_2$ X=H, phenyl, and p-nitro phenyl; see Scheme 2. In the first mechanism, Scheme 1 was adopted, as experimentally proposed by AL-AWADI (direct method). The second mechanism (Scheme 3) involved the formation of dimers. Later, these were modeled in accordance with the formation of a transition state according to the final products found experimentally. The third mechanism involved an initial four-membered cyclic transition state and an intermediate and six-membered cyclic transition state leading to product formation; Scheme 4.



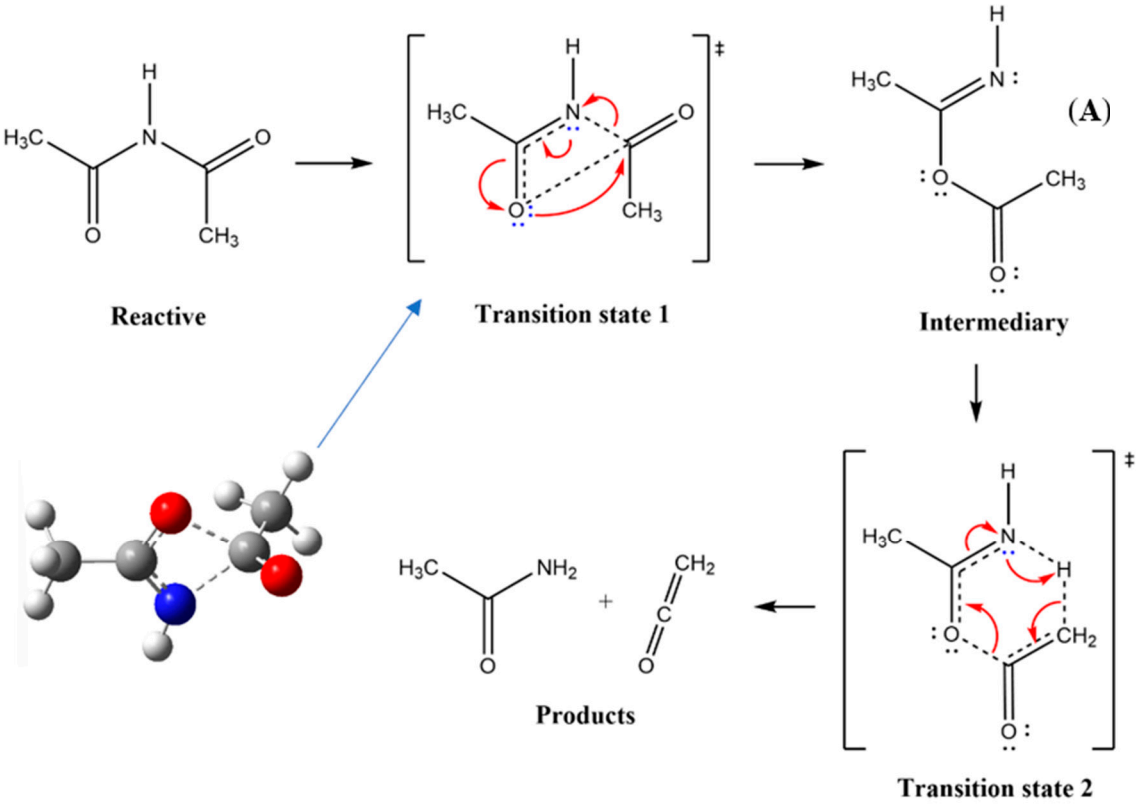
Scheme 2. Compounds studied in this work. R-N–[X=H (**A**), Phenyl (**B**), and p-nitro Phenyl (**C**)].



Scheme 3. Dimer formation $[NX(COCH3)_2$ X=H (A), phenyl (B)], Cl (C)$]_2$.

In dimers, hydrogens are transferred from both molecules and not from one in an intramolecular form. Calculations were performed at the X3LYP/def2TZVP level. The choice of this model will be seen later when we attack the direct mechanism of diacetamide breakdown. For the case of X=H, the calculation shows a dimer with an oscillation frequency of -1459.79 cm^{-1}, typical of a hydrogen vibration, with an enthalpy of -723.385921 Ha, which, with respect to the minimum energy monomer -361.731421 Ha, would yield an activation enthalpy of 201.96 kJ/mol, which is quite high. It was just as high when the hydrogen atom was replaced by a more effective electron attractor such as chlorine—that is, X=Cl—and the same functional X3LYP. In this case, the enthalpy of the monomer would

be −821.262913 Ha; compared to −1642.441213 Ha for the formation of the transition state; this would imply spending 222.14 kJ/mol of energy, with an oscillation frequency of −1475.01 cm^{-1}. A similar result emerged when the phenyl group, X=phenyl, was used, obtaining an energy of 212.16 kJ/mol to form. The high calculated energy values led us not to use this model in the subsequent calculations.



Scheme 4. Four-member transitional state 1 and formation of an intermediary (**A**). The intermediate leads to a second transition state 2 of a six-membered ring structure, giving rise to final products.

In the case of the second model or mechanism, in Scheme 4, transition state 1 is modeled by placing two fragments perpendicularly. This would generate an intermediate state (A) prior to the formation of the products, that is, a cetene and an amide. The intermediate compound would involve a transitional state of a seven-member ring, as enclosed below, when products are formed.

Table 2 shows the computational results for the mechanism proposed for Scheme 4, with five functionals and four basis sets with different polarization functions in addition to the basis set of Ahlrichs def2-TZVP being used. The calculated thermodynamic parameters were consistent with the values found experimentally, even with signs of entropy. Among all, the functional B3PW91 showed a better agreement with the activation energy values.

At this point, it was decided to apply the direct mechanism for the case of $NX(COCH_3)_2$ X=H. Table 3 shows the calculation results for diacetamide (X=H), a basis set of Def2-TZVP. As can be seen, it was not possible to reconcile the results according to the experimentally obtained activation energy value of about 150 kJ/mol. However, the proposed mechanism was adequate when hydrogen was replaced by a chlorine or methyl atom. In the first case, it is possible that chlorine will donate electron density to the nitrogen, strengthening the N-Cl bond, which can help polarize the C=O and increase the attractive force of methyl alpha hydrogens. The calculated thermodynamic parameters were consistent with the values found experimentally, even with signs of entropy. In the case of methyl, there is an electron donor effect. The excellent results found for the functional X3LYP and basis set of def2-TZVP, highlighted in black in Table 3, led us to use this model in the case of dimers.

Table 2. Arrhenius parameters calculated for pyrolysis of $NX(COCH_3)_2$ X=H. Mechanism Scheme 4.

	Properties	ΔG (kJ/mol)	ΔS (J/Kmol)	Ea (kJ/mol)
	Basis Set			
B3Pw91	6-311+G(3df,2p)	163.67	−18.00	155.34
	6-311+G(3df,2p) *	164.30	−17.10	156.52
	def2-TZVP	165.00	−17.67	159.39
X3LYP	def2-TZVP	169.02	−17.77	163.35
	6-311+G(3df,2p)	167.83	−17.10	162.56
B1LYP	def2-TZVP	172.22	−17.66	166.62
	6-311+G(3df,2p)	171.19	−17.12	163.39
LC-BLYP	def2-TZVP	186.757	−18.00	180.95
	6-311+G(3df,2p)	185.84	−17.94	177.55
CAM-B3LYP	def2-TZVP	176.625	−17.70	175.99
	6-311+G(3df,2p)	175.65	−17.24	167.78
ωB97X-D	def2-TZVP	177.733	−18.16	171.84
M062-X	def2-TZVP	175.415	−13.72	172.17

* Including a d3bj dispersion correction with Becke–Johnson damping.

Table 3. Arrhenius parameters calculated for pyrolysis of $NX(COCH_3)_2$ X=H with def2-TZVP basis set and several functionals. Mechanism Scheme 1.

Properties.	ΔG (kJ/mol)	ΔS (J/Kmol)	Ea (kJ/mol)
Experimental	165.05	−31.23	154.0
X3LYP	189.00	−14.00	185.61
ωB97X-D	201.96	−10.55	200.62
M062-X	191.44	−6.57	192.49
LC-BLYP	216.88	−8.13	216.99
CAM-B3LYP	199.59	−11.61	202.61
B3PW91	187.67	−11.53	185.75
B1LYP	192.30	−14.88	188.37
$NX(COCH_3)_2$ X=Cl			
X3LYP	158.04	−15.30	153.85
	(158.02) *	(−17.07) *	(152.75) *
B1LYP	161.95	−15.61	157.58
$NX(COCH_3)_2$ X=CH_3			
B1LYP	167.82	−7.07	168.57

* Using a 6-311+G(3df,2p) Pople basis set.

For the N-phenyl diacetamide (X=phenyl), our computational calculations show that the phenyl group is oriented perpendicular to the plane C(O)NC(O). This conformation prevents electron delocalization with the aromatic ring; regardless of whether the phenyl group is substituted with electron-withdrawing or electron donor groups, the experimental activation energy (Table 1) is approximately 30% of the value compared to hydrogen. In order to explain these values and demonstrate that nitrogen cannot share its electron pair with the phenyl ring, we proposed different actions. In the first place, we found three energetically probable conformers, with three possible methyl orientations (Figure 2); once the most stable structure was obtained (Figure 2C), the phenyl was rotated in 10° inter-

vals from 90 to 180°. We calculated its charge, intrinsic bond strength index (IBSI), and energy change when the phenyl orientation was modified from perpendicular to in-plane orientations. The results are shown in Table 4.

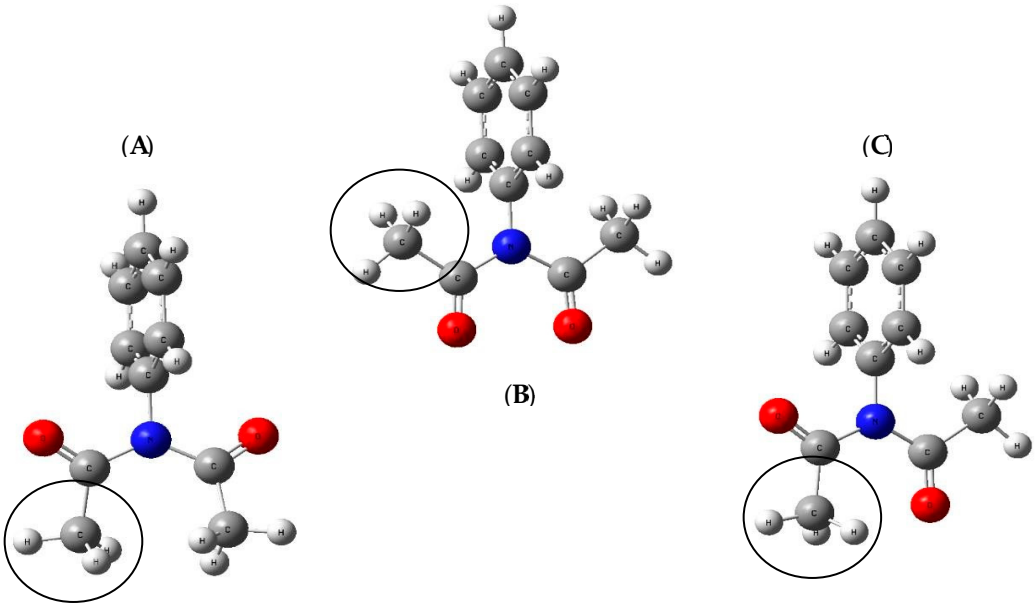


Figure 2. (**A**) Methyl groups facing each other (E: −592.407279 ha); (**B**) head-to-head ketones (E: −592.408915 Ha); (**C**) ketone–methyl face to face (E: −592.417458 Ha). All calculations were performed with B1LYP/6-31+G(d,p).

Table 4. NBO and IBSI from 90° to 180°, corresponding to the aromatic ring perpendicular to or coplanar to the C(O)NC(O) plane at the B3PW91/6-311+G(3df,2p) level of theory.

Tipo	**Degrees**									
	90	100	110	120	130	140	150	160	170	180
Labels	**NBO charges**									
N1	−0.557	−0.557	−0.556	−0.554	−0.552	−0.551	−0.550	−0.549	−0.550	−0.551
C14	0.152	0.152	0.150	0.150	0.150	0.150	0.151	0.150	0.153	0.154
Bond	**IBSI**									
N1-C14	1.099	1.109	1.135	1.159	1.181	1.210	1.211	1.224	1.252	1.272
	NBO charges									
C2	0.715	0.715	0.714	0.714	0.714	0.715	0.716	0.721	0.728	0.737
Bond	**IBSI**									
N1-C2	1.204	1.203	1.201	1.194	1.185	1.170	1.150	1.120	1.081	1.048
	NBO charges									
C7	0.721	0.721	0.722	0.722	0.722	0.722	0.721	0.719	0.715	0.708
Bond	**IBSI**									
N1-C7	1.192	1.192	1.192	1.196	1.199	1.199	1.203	1.214	1.234	1.265

Any attempt to place the aromatic ring in the same plane as C(O)NC(O) was rendered impossible. To calculate the energy cost, a redundant coordinate calculation was made in which the torsional barrier (TB) was determined. These calculations were performed at the B3PW91/6-311+G(3df,2p) level of theory.

To determine the torsional barrier (TB), the conformation scans started with the phenyl perpendicular ring to the plane C(O)NC(O), shown in structure A with an angle of 90.06° and energy of −592.92 Ha, and ended with the phenyl ring rotated at 180° with respect to the initial conformation. In the final conformation, shown in structure B, the phenyl ring is coplanar to the plane C(O)NC(O) and the energy is −592.90 Ha. The energy change difference is 39.96 kJ/mol. The result is shown in Figure 3, along with the total energy

scanned. The atom numbers in structure A of Figure 3 depict the atom numbering for the NBO calculation. The IBSI parameters are shown in Table 4.

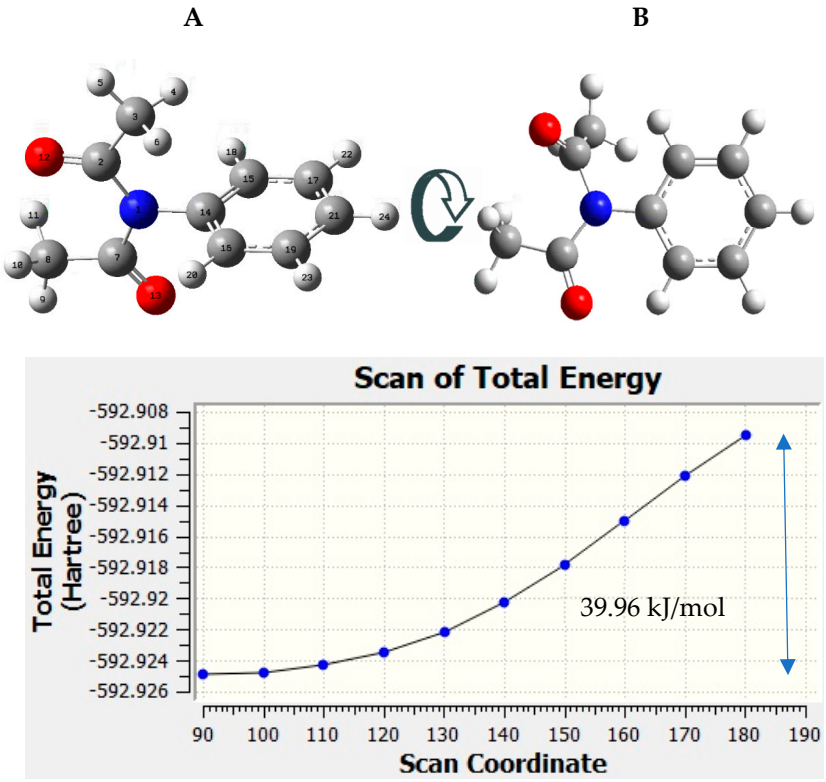


Figure 3. Scanned potential surface of two structures at the B3PW91/6-311+G(3df,2p) level of theory. (**A**) Reactant; (**B**) reactant after phenyl rotation.

Figure 4 now shows the potential energy surface resulting from the rotation of two dihedral scan coordinates (SC1: C2-N1-C14-C15 and SC2: C14-N1-C2-C3; see Figure 3A for the atom labels) and the results from the additional movement of the groups of atoms attached to the nitrogen atom. The figure shows two black arrows; with the top one, the transition state is observed, and the one below corresponds to the global minimum found. When taking the difference in energies between these points (591.533275–591.461992) Ha, it corresponds to 187.15 kJ/mol, which is very close to the value measured experimentally. The IBSIs, in Table 4, show that when the benzene ring was coplanar to the C(O)NC(O) plane, electron density shifted from the aromatic ring towards the carbonyl carbon. That effect is not appreciable when the ring is perpendicular to the C(O)NC(O) plane. A slight displacement of the NBO charges by the ring can also be seen at the N1-C14 bond of contribution when the system is in the C(O)NC(O) plane. Table 5 shows the thermodynamic parameters using the functional B3PW91. The best agreement was found when X=hydrogen. Close attention was paid to two variables: the sign of entropy and the value of the activation energy.

As can be seen in Table 5, the Pople basis set 6-31G and functional B3Pw91 generate the value of 186.95 kJ/mol, which is very close to the experimental one. However, it is observed that the entropy has a positive value of 17.61 J/K.mol. When we improve the basis sets and add a polarization function (d), the entropy changes to negative and the activation energy drops to 178.07 kJ/mol. Nonetheless, considering the experimental error, this was a better value. The entropy value decreases as the basis sets improve. When using the B1LYP functional, we found something interesting; the results converge very well, but they worsen as the basis set size is increased. This induced us to investigate whether there was a basis set superposition error (BSSE) effect [27] since in the transition state, two molecules are separated. This basis effect was calculated to avoid the underestimation of the results.

From Table 5, it is clear that BBSE correction did not result in a significant change (only about 6 kJ/mol); consequently, we did not continue using it.

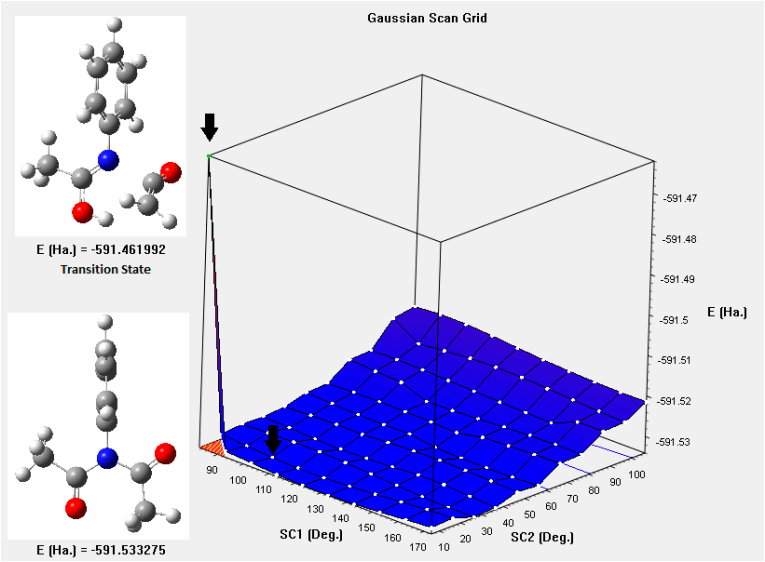


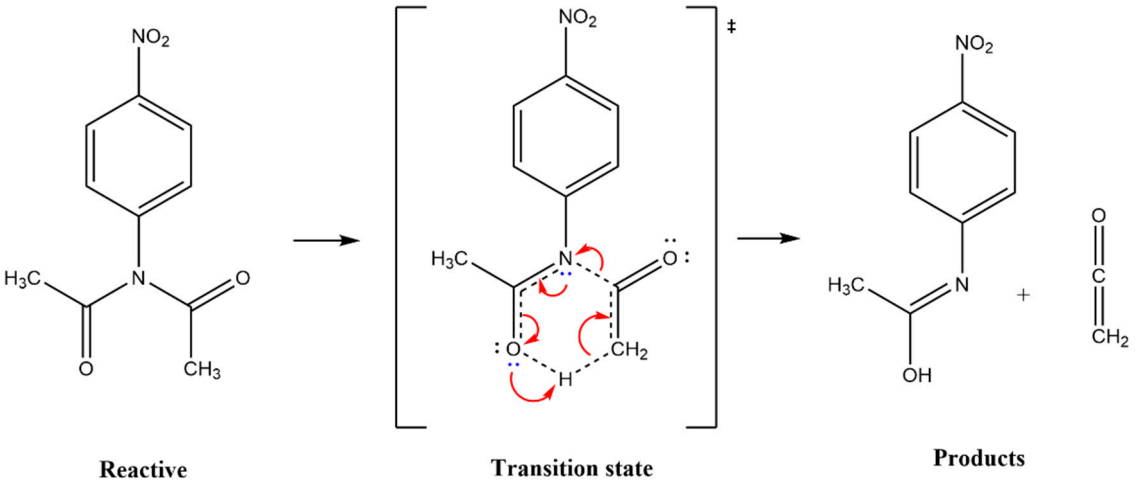
Figure 4. Potential energy surface $NX(COCH_3)_2$ X = phenyl, with the functional LC-BLYP and def2-TZVP basis set, using the Gaussian16 scan grid option with two dihedral scan coordinates. (SC1: C2-N1-C14-C15 and SC2: C14-N1-C2-C3; see Figure 3A for the atom labels.

Table 5. Arrhenius parameters calculated for pyrolysis of $NX(COCH_3)_2$ X=phenyl. Mechanism Scheme 1.

Parameters	ΔG (kJ/mol)	ΔS (J/Kmol)	Ea (kJ/mol)
Experimental	189.11	−14.00	185.70
	B1LYP		
6-31G	175.79	−1.51	177.36
6-311G	167.19	−5.34	166.46
6-31G(d,)	178.14	−7.17	176.31
6-31+G(d)	175.14	−7.38	173.19
6-31G+G(d,p)	161.58	−5.81	160.57
6-31G+G(d,p) BSSE	168.46	−7.88	166.21
def2-TZVP	160.79	−22.36	152.37
	B3Pw91		
6-31G	171.39	17.61	186.95
6-31G(d)	173.54	−0.76	178.07
6-311+G(2d,2p)	154.48	1.36	160.29
6-311+G(3df,2p)	151.98	3.27	156.42
	LC-BLYP		
def2-TZVP	183.98	−4.14	186.48

In the case of 4-nitrophenyl, in Scheme 5, as has been shown for the case of the phenyl group when the ring is perpendicular to the plane of the C(O)NC(O), the electron-withdrawing or electron donor group has no appreciable effect on the reaction rate. In fact, when phenyl is used, the value of the experimentally calculated activation energy is 185.7 (± 7.5) kJ/mol, and compared to 4-nitrophenyl, this value is 192 kJ/mol, which

is the same as within the experimental error. To prove this assertion, we calculated the activation energy at the B3PW91 level of theory (including a dispersion correction with Becke–Johnson damping (d3bJ) and the 6-311+G(3df,2p) basis set).



Scheme 5. Nitrophenyl diacetyl amine until product formation.

The calculation of the thermodynamic properties at the B3PW91-D3BJ/6-311+G(3df,2p) level of theory yields an activation energy value of 150.69 kJ/mol, a value that is comparable to that calculated for the case of phenyl at 156.52 kJ/mol. Regarding the entropy change of −8.64 J/K mole, its value was consistent with a negative value. All the above results allow us to infer that the reaction mechanism is the same as for *N*-phenyl, a direct mechanism. An even better result is obtained using the functional LC-BLYP and the def2-TZVP basis set.

Table 6 shows the thermodynamic results maintaining the base set def2-TZVP and varying the type of functional. A correspondence between the calculated and experimental energy of activation was observed when using the LC-BLYP/def2-TZVP level of theory; that is, this functional provides the best description of our system and shows that it does not matter in which position the nitro group is located to characterize the displacement of the electrons towards the aromatic ring.

Table 6. Arrhenius parameters calculated for pyrolysis of NX(COCH3)2 X=nitro diacetamide. Mechanism Scheme 1 with def2-TZVP.

Parameters	ΔG (kJ/mol)	ΔS (J/Kmol)	Ea (kJ/mol)
Experimental	189.11	−14.00	185.70
	p-nitro		
X3LYP	157.110	−22.97	148.32
B3Pw91	294.038	−11.32	292.26
LC-BLYP	182.877	−8.92	182.51
	m-nitro		
X3LYP	158.176	−24.66	148.38
B3Pw91	294.636	−9.67	293.83
LC-BLYP	183.113	−7.49	183.61

In addition to the case of the phenyl, the case of 4-nitrophenyl offered an opportunity to explore some of the features of the natural bond analysis (NBO) for studying both inter- and intramolecular interactions, as well as interactions between bonds, charge transfers, or conjugative interactions in molecular systems. In fact, the NBO method gives very

useful information about the interactions between full and empty orbitals, which is equally important in the reactivity of interacting systems. This last feature is accomplished by considering all possible interactions between natural bond orbitals (NBOs), donors, and acceptors and then estimating their involved energies using second-order perturbation theory [28]. For each donor orbital (i), there is an acceptor orbital (j), and the associated stabilization energy $E(2)$, due to the electronic delocalization, is given by

$$E(2) = \Delta E_{i,j} = \frac{q^i F(i,j)}{(E_j - E_i)} \quad (3)$$

where q^i is the occupation of the orbital, i.e., the number of electrons, E_j and E_i are the energies involved and $F(i,j)$ are the elements outside the diagonal of the Fock matrix. In this sense, a great value of $E(2)$ is indicative of the intensity of the interaction between the electron-donor and electron-acceptor species, meaning that there is a greater tendency for electrons to be donated and, therefore, a greater conjugation of the studied system.

For our case, natural bond orbital analysis was performed using the B3PW91/6-311+G(3df,2p) d3bj method. For the specific case of the 4-nitrophenyl diacetamide, shown in Figure 5, several points of the IRC graph of Figure S6 were studied, passing the structure from a reactant to the products. Here, we selected the bonds N1-C14, N1-C7, C7-O13, and C21-N24. Such bonds would show the path of the electrons or the conjugation that could be present. Figure S6 is formed by 34 points before the transition state and 40 points from then, up to the formation of the products. There, we selected some optimized structures and constructed Table 7. It shows the strong interaction of N1 electrons towards the C7-O13 bond; this electron migration favors the extraction of hydrogen β. During this process, it is also observed that before reaching the transition state, no involvement of the lone electron pairs of nitrogen is observed. After the transition state, the IBSI value for the N1-C2 bond is not displayed, as it is less than 0.05. Within the nitro group, there is a strong conjugation above 170 a.u. for the value of the perturbation energy. A total of eight structures or points were studied, including the transition state. IBSI values for the N1-C14 and N24-C21 bonds remained constant during the mechanistic process. These results reinforce the non-conjugate participation of the benzene ring, and, therefore, the reaction rate would not be affected by the presence of the nitro group in the phenyl. The NBO was included in the Gaussian16 package and the IBSIs were calculated using the IGMPLOT program.

Table 7. NBO analysis of the IRC Fock matrix and IBSI values for 4-nitrophenyl diacetamide at the B3PW91/6-311+G(3df,2p) level of theory with dispersion correction and Becke–Johnson damping (d3bj). BST is before, ST is during, and ATS is after the transition state, respectively.

Point	Donor NBO (i)	Acceptor NBO (j)	E (2) kcal/mol	IBSI			
				N1-C2	N1-C7	N1-C14	N24-C21
01 (BTS)	LP (1)N1	BD*(2) C2-O12	15.70	1.030			
	LP (1)N1	BD*(1) C14-C15	4.75			1.216	
	LP (3)O26	BD*(2) N24-O25	173.79				1.105
02	LP (1)N1	BD*(2) C2-O12	14.88	0.991			
	LP (1)N1	BD*(1) C14-C15	4.88			1.227	
	LP (3)O26	BD*(2) N24-O25	173.63				1.105
03	LP (1)N1	BD*(2) C2-O12	12.45	0.877			
	LP (1)N1	BD*(1) C14-C15	5.02			1.238	
	LP (3)O26	BD*(2) N24-O25	173.51				1.104

Table 7. *Cont.*

Point	Donor NBO (i)	Acceptor NBO (j)	E (2) kcal/mol	IBSI			
				N1-C2	N1-C7	N1-C14	N24-C21
04	LP (1)N1	BD*(2) C2-O12	10.26	0.787			
	LP (1)N1	BD*(1) C14-C15	4.94			1.245	
	LP (3)O26	BD*(2) N24-O25	173.6				1.102
(ST)	LP (1)N1	BD*(1) C7–C8	9.75		1.621		
	LP (1)N1	BD*(2) C14-C16	16.81			1.293	
	LP (3)O26	BD*(2) N24-O25	172.62				1.107
06 (ATS)	LP (1)N1	BD*(1) C7-O13	8.62		1.689		
	LP (1)N1	BD*(1) C14-C15	19.04			1.328	
	LP (3)O26	BD*(2) N24-O25	170.83				1.120
07	LP (1)N1	BD*(1) C7-O13	8.86		1.692		
	LP (1)N1	BD*(1) C14-C15	19.22			1.325	
	LP (3)O26	BD*(2) N24-O25	170.69				1.120
08	LP (1)N1	BD*(1) C7-O13	9.09		1.692		
	LP (1)N1	BD*(1) C14-C15	19.30			1.317	
	LP (3)O26	BD*(2) N24-O25	170.59				1.120

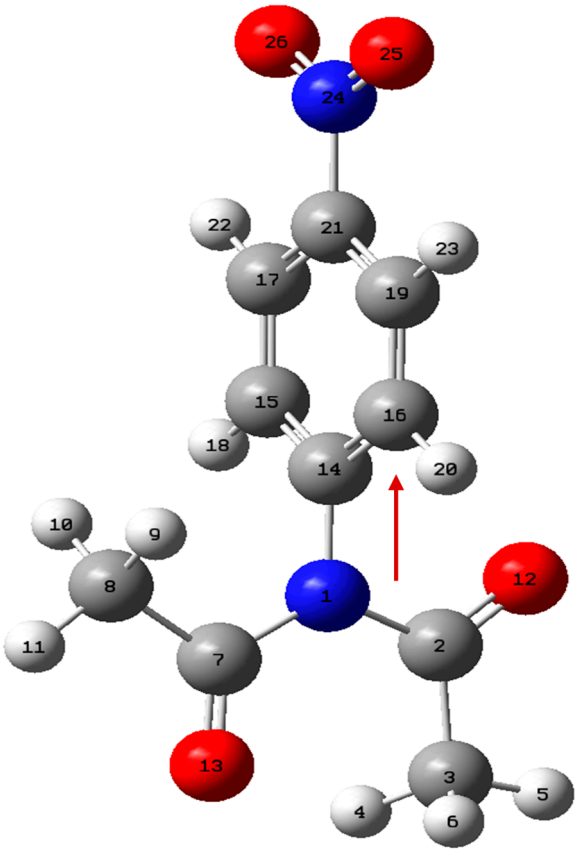


Figure 5. Possible migration of electrons due to the presence of the nitro group in benzene.

Bond orders can also be used as descriptors of covalent bonding, involving two atoms, and they are used very widely in chemistry. Indeed, notions of single, double, and triple bonds (with bond orders of 1, 2, and 3, respectively) are very common. In this work, attention was paid to the binding between the groups (X=H, phenyl, or Cl) and nitrogen, in search of any modification of the electron density. In particular, the Mayer bond order is a natural extension of the Wiberg bond order, which has been proven extremely useful in bonding analysis using semi-empirical computational methods and Mulliken population analysis to develop ab initio theories. Figure 6 shows a Mayer bond order analysis for the case of $NX(COCH_3)_2$ X=H, phenyl, and Cl. Most details can be visualized in the Supplementary Materials. The biggest contributor to the bond strength is the Chloro group followed by the phenyl group. In the case of X, when it is replaced by hydrogen, there is not much of a change noticed—only during the transition state.

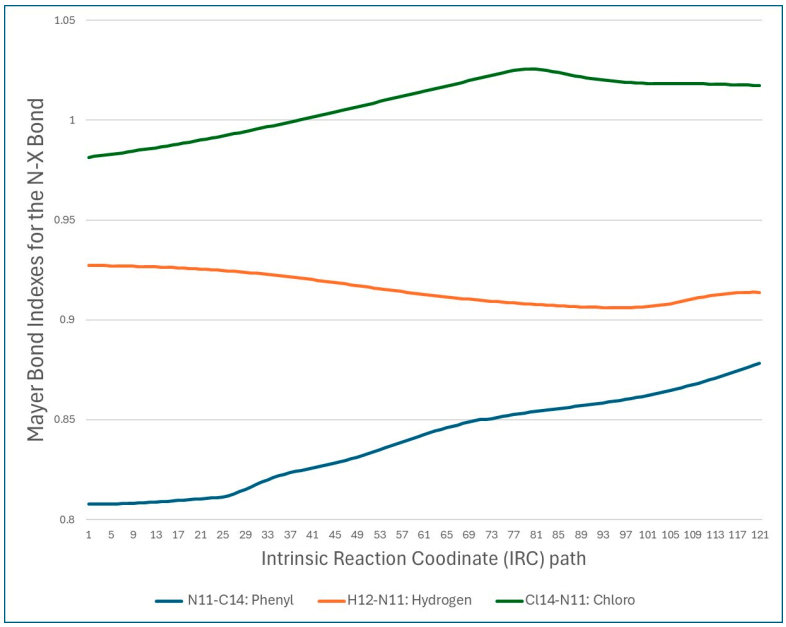


Figure 6. Mayer bond order indexes (*y*-axis) for the $NX(COCH_3)_2$ X=H, phenyl, and Cl at the LC-BLYP/def2-TZVP level of theory from an IRC calculation.

4. Conclusions

The calculations carried out during this work allowed us to identify and study different types of reaction mechanisms from the one proposed in the experimental study by AL-AWADI involving a six-membered ring. In that proposal, the participation of the lone electron pair of nitrogen played an important role, assuming delocalization effects by aromatic substituents at the nitrogen atom. However, it was not possible to use the same mechanism for all molecules studied. Several mechanisms were suggested depending on the substituents present. When at $NX(COCH_3)_2X$, we substituted X=H; the calculated activation energies suggested a two-stage mechanism, different from the case of X=phenyl, where the best agreement between experimental and calculated parameters led to one direct mechanism at which the phenyl was almost perpendicular to the C(O)NC(O) plane. A small rotational energy barrier of 39.96 kJ/mol was sufficient to prevent the electron delocalization between the nitrogen and the aromatic ring, thereby explaining the negligible effect of the ring substituent in the reaction rates.

Supplementary Materials: The following supporting information can be downloaded at https://www.mdpi.com/article/10.3390/molecules29163833/s1: Figure S1: IRC calculation from reactant to products at theory level B3PW91/6-311+G(3df,2p) gd3bj. Figure S2: Dimer proposal for the case of diacetamide NX(COCH3)2 X=H. (A) Monomer; (B) dimer; (C) IRC: intrinsic reaction for the double-hydrogen migration. Model is discussed in the main manuscript. Theory level: X3LYP/def2-TZVP. Scheme SS1: Final step-path of the dimer formation Scheme 3 (main manuscript). Table ST1: Wiberg Indexes for the Phenyl-diacetamide/LC-BLYP-def2-TZVP. Figure S3: Phenyl–diacetamide at the LC-BLYP– def2-TZVP level of theory. (A) Atomic label, (B) NBO charges (reactant), (B) NBO charges for the transition state (TS), and (D) NBO charges for the product. Table ST2: Wiberg indexes for the Diacetamide/B3PW91–d3bj-def2-TZVP-Fisrt Stage. Figure S4: Diacetamide at the level of theory B3PW91-d3bj-def2-TZVP. (A) Atomic label, (B) NBO charges (reactant). (C) NBO charges (Transition State), (D) NBO charges (product). Table ST3: Wiberg indexes for the Diacetamide/B3PW91–d3bj-def2-TZVP-Second Stage. Figure S5: Diacetamide at the level of theory B3PW91-d3bj-def2-TZVP. (A) NBO charges (Transition State), (C) NBO charges (product). Figure S6: Mayer bond order analysis for phenyl–diacetamide at the LC-BLYP–def2-TZVP level of theory with data from an IRC calculation. Figure S7: Mayer bond order analysis for the diacetamide at the LC-BLYP–def2-TZVP level of theory with data from an IRC calculation. Figure S8: Mayer bond order analysis for the Chloro-diacetamide at the LC-BLYP–def2-TZVP level of theory with data from an IRC calculation. Figure S9: IBSI diagrams for phenyl–diacetamide at the LC-BLYP–def2-TZVP level of theory with data from an IRC calculation. Figure S10: IBSI diagrams for diacetamide at the LC-BLYP–def2-TZVP level of theory with data from an IRC calculation. Figure S11: IBSI diagrams for chloro–diacetamide at the LC-BLYP–def2-TZVP level of theory with data from an IRC calculation.

Author Contributions: Conceptualization, M.L.; Methodology, O.G.T. and M.L.; Software, O.G.T. and M.L.; Validation, J.L.P. and T.C.-S.; Investigation, O.G.T. and M.L.; Resources, A.G.S.; Writing—original draft, M.L.; Writing—review & editing, J.L.P., T.L.F. and T.C.-S.; Supervision, M.L.; Funding acquisition, A.G.S. All authors have read and agreed to the published version of the manuscript.

Funding: This research received no external funding.

Institutional Review Board Statement: Not applicable.

Informed Consent Statement: Not applicable.

Data Availability Statement: Any data not presented in the link provided in the supplementary materials section, can be available on request from the corresponding authors.

Acknowledgments: The authors would like to thank the DEINPRO group for the use of the computer equipment. Likewise, to the Faculty of Chemistry and Chemical Engineering and the Universidad Nacional Mayor de San Marcos for the use of the physical spaces.

Conflicts of Interest: The authors declare no conflicts of interest.

References

1. Soheil, M.; Alireza, F. *Encyclopedia of Toxicology*, 4th ed.; Wexler, P., Ed.; Academic Press: Cambridge, MA, USA, 2024; pp. 39–42. [CrossRef]
2. Kuroda, Y.; Saito, Y.; Machida, K.; Uno, T. Infrared dichroism and out-of-plane vibrations of trans-cis diacetamide and its C- and N-deuterated derivatives. *Spect. Acta Part A Mol. Spectrosc.* **1973**, *29*, 411–421. [CrossRef]
3. Kuroda, Y.; Saito, Y.; Machida, K.; Uno, T. Infrared spectra of trans-cis diacetamide and its C- and Ndeuterated compounds. *Spectrochim. Acta Part A Mol. Spectrosc.* **1971**, *27*, 1481–1493. [CrossRef]
4. Gallaher, K.L.; Batter, S.H. Structure of diacetamide. Reference amido structures for polypeptide conformation analysis. *J. Chem. Soc. Faraday Trans. 2* **1975**, *71*, 1423–1435. [CrossRef]
5. Ramondo, F.; Nunziante Cesaro, S.; Bencivenni, L. Effects of intermolecular hydrogen bonding on the molecular structure and vibrational spectrum of diacetamide. *J. Mol. Struct.* **1993**, *291*, 219–244. [CrossRef]
6. Matias, P.M.; Jeffrey, G.A.; Ruble, J.R. Structures of the *E*,*Z* (*cis–trans*) isomer of diacetamide and the 1:1 complex with acetamide at 123 K. Ab-initio molecular orbital calculations on the *Z*,*Z* (*trans–trans*), *E*,*Z* (*cis–trans*) and *E*,*E* (*cis–cis*) isomers of diacetamide. *Acta Cryst. Sect. B Struct. Sci.* **1988**, *44*, 516–522. [CrossRef]
7. Altarawneh, M.; Altarawneh, K. A theoretical study on the bimolecular reactions encountered in the pyrolysis of acetamide. *J. Phys. Org. Chem.* **2012**, *25*, 431–436. [CrossRef]

8. Hurd, C.D. *The Pyrolysis of Carbon Compounds*; ACS Monograph Series No. 50; The Chemical Catalog Co., Ltd.: New York, NY, USA, 1929.
9. Irwin, W.J. Analytical pyrolysis an overview. *J. Anal. Appl. Pyrolysis* **1979**, *1*, 89–122. [CrossRef]
10. Ericsson, I.; Lattimer, R. Pyrolysis nomenclature. *J. Anal. Appl. Pyrol.* **1989**, *14*, 219–221. [CrossRef]
11. Uden, P. Nomenclature and terminology for analytical pyrolysis (IUPAC Recommendations 1993). *Pure Appl. Chem.* **1993**, *65*, 2405–2409. [CrossRef]
12. Almeida-Neto, F.W.Q.; Matos, M.G.C.; Marinho, E.M.; Marinho, M.M.; Sampaio, T.L.; Bandeira, P.N.; Dos Santos, H.S. In silico study of the potential interactions of 4′-acetamidechalcones with protein targets in SARS-CoV-2. *Biochem. Biophys. Res. Commun.* **2021**, *537*, 71–77. [CrossRef]
13. Hariyono, P.; Dwiastuti, R.; Yusuf, M.; Salin, N.H.; Hariono, M. 2-Phenoxyacetamide derivatives as SARSCoV-2 main protease inhibitor: In silico studies. *Results Chem.* **2022**, *4*, 100263. [CrossRef] [PubMed]
14. Moldoveanu, S. *Pyrolysis of Organic Molecules with Applications to Health and Environment*; Techniques and Instrumentation in Analytical Chemistry; Elsevier: Amsterdam, The Netherlands, 2010; Volume 28, pp. 1–724. Available online: https://www.sciencedirect.com/bookseries/techniques-and-instrumentation-in-analytical-chemistry/vol/28/suppl/C (accessed on 5 August 2024).
15. Al-Awadi, N.A.; Al-Omran, F.A. Gas-phase kinetics of N-substituted diacetamide. *Int. J. Chem. Kinet.* **1994**, *26*, 951–954. [CrossRef]
16. Frisch, M.J.; Trucks, G.W.; Schlegel, H.B.; Scuseria, G.E.; Robb, M.A.; Cheeseman, J.R.; Scalmani, G.; Barone, V.; Petersson, G.A.; Nakatsuji, H.; et al. *Gaussian 16*, revision C.01-version 1.1; Gaussian, Inc.: Wallingford CT, USA, 2016.
17. G09 Keywords: DFT Methods. Available online: http://www.chemistry4.me/gaussian/g09w/help/g09/l_keywords09.htm (accessed on 5 August 2024).
18. Schuchardt, K.L.; Didier, B.T.; Elsethagen, T.; Sun, L.; Gurumoorthi, V.; Chase, J.; Li, J.; Windus, T.L. Basis Set Exchange: A Community Database for Computational Sciences. *J. Chem. Inf. Model.* **2007**, *47*, 104552. [CrossRef] [PubMed]
19. Lu, T.; Chen, F. Multiwfn: A multifunctional wavefunction analyzer. *J. Comput. Chem.* **2012**, *33*, 580–592. [CrossRef] [PubMed]
20. Lefebvre, C.; Rubez, G.; Khartabil, H.; Boisson, J.C.; Contreras-García, J.; Hénon, E. Accurately extracting the signature of intermolecular interactions present in the NCI plot of the reduced density gradient versus electron density. *Phys. Chem. Chem. Phys.* **2017**, *19*, 17928–17936. [CrossRef] [PubMed]
21. Lefebvre, C.; Khartabil, H.; Boisson, J.C.; Contreras-García, J.; Piquemal, J.P.; Hénon, E. Independent Gradient Model: A new approach for probing strong and weak interactions in molecules from wave function calculations. *Chem. Phys. Chem.* **2018**, *19*, 724–735. [CrossRef] [PubMed]
22. Ponce-Vargas, M.; Lefebvre, C.; Boisson, J.C.; Hénon, E. Atomic Decomposition Scheme of Noncovalent Interactions Applied to Host–Guest Assemblies. *J. Chem. Inf. Model.* **2020**, *60*, 268–278. [CrossRef] [PubMed]
23. Klein, J.; Khartabil, H.; Boisson, J.C.; Contreras-García, J.; Piquemal, J.P.; Hénon, E. New Way for Probing Bond Strength. *J. Phys. Chem. A* **2020**, *124*, 1850–1860. [CrossRef]
24. Lefebvre, C.; Khartabil, H.; Hénon, E. New insight into atomic-level interpretation of interactions in molecules and reacting systems. *Phys. Chem. Chem. Phys.* **2023**, *25*, 11398–11409. [CrossRef]
25. Lefebvre, C.; Klein, J.; Khartabil, H.; Boisson, J.; Hénon, E. IGMPlot: A program to identify, characterize, and quantify molecular interactions. *J. Comput. Chem.* **2023**, *44*, 1750–1766. [CrossRef]
26. McQuarrie, D. *Statistical Mechanics*; Harper & Row: New York, NY, USA, 1986.
27. Tzeli, D.; Tsekouras, A.A. Mind the basis set superposition error. *Chem. Phys. Lett.* **2010**, *496*, 42–45. [CrossRef]
28. Reed, A.E.; Curtis, L.A.; Weinhold, F. Intermolecular interactions from a natural bond orbital, donor-acceptor viewpoint. *Chem. Rev.* **1988**, *88*, 899–926. [CrossRef]

Disclaimer/Publisher's Note: The statements, opinions and data contained in all publications are solely those of the individual author(s) and contributor(s) and not of MDPI and/or the editor(s). MDPI and/or the editor(s) disclaim responsibility for any injury to people or property resulting from any ideas, methods, instructions or products referred to in the content.